Compact Packing of Lipocalin-type Prostaglandin D Synthase Induced by Binding of Lipophilic Ligands*

Katsuaki Inoue[1], Naoto Yagi[1], Yoshihiro Urade[2] and Takashi Inui[3,4,†]

[1]*Research & Utilization Division, Japan Synchrotron Radiation Research Institute, 1-1-1 Koto, Sayo, Hyogo 679-5198;* [2]*Department of Molecular Behavioral Biology, Osaka Bioscience Institute, 6-2-4 Furuedai, Suita, Osaka 565-0874;* [3]*Laboratory of Protein Sciences, Graduate School of Life and Environmental Sciences, Osaka Prefecture University, 1-1 Gakuen-cho, Naka-ku, Sakai, Osaka 599-8531; and* [4]*Department of Food and Nutrition, Tsu City College, 157 Ishinden-Nakano, Tsu, Mie 514-0112, Japan*

Lipocalin-type prostaglandin (PG) D synthase (L-PGDS) is a multi-functioning protein belonging to the lipocalin family, acting as a PGD_2-synthesizing enzyme and as an extracellular transporter for small lipophilic molecules. In the present study, to clarify the conformational changes of lipocalin proteins induced by binding of lipophilic ligands, such as all-*trans*-retinoic acid (RA), bilirubin (BR) and biliverdin (BV), we measured small-angle X-ray scattering (SAXS) of L-PGDS and that of two other lipocalins, β-lactoglobulin (βLG) and retinol-binding protein (RBP). L-PGDS bound all three ligands with high affinity, while βLG and RBP could bind only RA. The radius of gyration was estimated to be 19.4 Å for L-PGDS, and 18.8 Å for L-PGDS/RA, 17.3 Å for L-PGDS/BR and 17.8 Å for L-PGDS/BV complexes, indicating that L-PGDS became compact after binding of these ligands. Alternatively, the radius of gyration of βLG and RBP was 20.3 and 26.2 Å, respectively, and was almost the same before and after RA binding. Based on the SAXS data, we found that the compact packing upon binding ligands is a special feature of L-PGDS and it may be ascribed to the conformational flexibility of L-PGDS molecule itself, which underlies the high-affinity for its ligands.

Key words: broad selectivity, compact packing, conformational change, radius of gyration, SAXS.

Abbreviations: βLG, β-lactoglobulin; BR, bilirubin; BV, biliverdin; K_d, dissociation constant; L-PGDS, lipocalin-type prostaglandin D synthase; PG, prostaglandin; RA, all-*trans*-retinoic acid; RBP, retinol-binding protein; R_g, radius of gyration; SAXS, small-angle X-ray scattering.

Lipocalin-type prostaglandin D synthase (L-PGDS; prostaglandin-H_2 D-isomerase, EC 5.3.99.2) is responsible for the biosynthesis of prostaglandin D_2 (PGD_2) from prostaglandin H_2, which is a common precursor of all prostanoids (*1*). L-PGDS is also known as a member of the lipocalin superfamily (*2*), which comprises lipid-transporter proteins such as β-lactoglobulin (βLG), retinol-binding protein (RBP), major urinary protein, aphorodisin and tear lipocalin (*3–6*). It is well known that the lipocalins are small proteins of approximately 200 amino acid residues and 20 kDa in the molecular weight. Their tertiary structures are closely similar in spite of their wide range of functions and high levels of sequence divergence (*3*). That is, the lipocalin proteins have a highly symmetrical all-β structure dominated by a single eight-stranded antiparallel β-sheet closed back on itself to form a continuously hydrogen bonded β-barrel (*7*, *8*). This β-barrel commonly encloses a ligand-binding site composed of both an internal cavity and an external loop scaffold (*3*). So far, we have clarified that L-PGDS can act not only as an enzyme but also as a lipid transporter (*9–12*). The results of such studies also revealed that L-PGDS can bind a large variety of lipophilic ligands, such as retinoids, biliverdin, bilirubin, thyroid hormones, gangliosides and amyloid beta peptides *in vitro* (*10–14*) with high-binding affinity. We defined such a feature as its 'broad ligand selectivity' (*15*). However, in contrast to the extensive data obtained on L-PGDS from many biochemical studies, detailed information about the conformational changes that it undergoes when it forms a complex with a ligand still remains to be forthcoming. It is essential to know the molecular structure of L-PGDS itself in order to understand the origin of the features of L-PGDS. Generally, to clarify the molecular structure of proteins at the atomic level, X-ray crystallography or NMR is indispensable and should be adopted. However, X-ray crystallographic studies on L-PGDS/ligand complexes have not proceeded because of failure to crystallize them. The NMR studies on L-PGDS/ligand complexes also have not been successful, because of the obscure spectrum obtained from a solution of these complexes. Thus, in the present study, we measured the structure of L-PGDS and its complexes with three kinds of lipophilic ligands in solution by using the small-angle X-ray scattering (SAXS) method. SAXS is

a powerful technique for directly obtaining and characterizing the size, overall shape and compactness of molecules under solution conditions, and thus is particularly useful for studying systems in which a structural or a conformational change takes place (*16*). Based on the SAXS data, we found that L-PGDS became compact upon binding a ligand. Such compact packing may lead to the high affinity for its ligands.

EXPERIMENTAL PROCEDURE

Chemicals—Thrombin, RA, BR, BV, bovine βLG-A and bovine RBP were purchased from Sigma Chemical Co. (St Louis, MO, USA). All other chemicals were of analytical grade.

Expression of Recombinant Mouse L-PGDS—The C65A-substituted recombinant mouse L-PGDS was expressed as a glutathione S-transferase fusion protein in *Escherichia coli* DH5α (TOYOBO, Tokyo, Japan) as described previously (*12*). The fusion protein was bound to glutathione-Sepharose 4B (GE Healthcare Bio-Sciences) and incubated with thrombin (Sigma Chemical Co., St Louis, MO, USA, 100 U/100 μl) to release the L-PGDS. This mutant protein, possessing an intact intrinsic disulfide bond, was employed instead of the native protein, which is limited in amount caused by forming incorrect disulfide bond. The protein was purified by using size exclusion chromatography as described earlier (*15*). Then, the purified protein was dialysed against 5 mM Tris/HCl (pH 8.0).

Fluorescence Quenching Assays—RA, BR and BV were each dissolved in DMSO to give a 2 mM stock solution. The concentrations were determined spectroscopically based on their respective molar absorption coefficients of ε_{453} in chloroform for BR (*17*) = 61,700 $M^{-1} cm^{-1}$, ε_{377} in methanol for BV (*18*) = 51,500 $M^{-1} cm^{-1}$ and ε_{336} in ethanol for RA (*19*) = 45,000 $M^{-1} cm^{-1}$. Various concentrations of each lipophilic ligand were added to L-PGDS, βLG or RBP in 5 mM Tris/HCl for pH 8.0, and the final concentration of each protein was adjusted to 1.5 μM. After incubation at 25°C for 30 min, the intrinsic tryptophan fluorescence was measured as described previously (*15*). The quenching of tryptophan fluorescence caused by non-specific interactions with each ligand was corrected with 1.5 μM *N*-acetyl-L-tryptophanamide. The dissociation constant (K_d) values for binding between various kinds of lipophilic ligands and L-PGDS, βLG or RBP were calculated by the method described earlier (*20*).

Preparation of L-PGDS Complexes—Purified L-PGDS was mixed with each ligand in a 1:1 molar concentration ratio. After 1 h of stirring, in order to remove ethanol or DMSO from the solvent and aggregates, the mixture was applied to a Superdex75 column (GE Healthcare BioSciences, Little Chalfont, UK); and only the fractions containing complexes were gathered. These fractions were then concentrated and adjusted to optimal concentrations (2.5–12.5 mg ml^{-1}).

SAXS Experiments—SAXS data were collected at the BL40B2 in the SPring-8 synchrotron radiation facility (Hyogo, Japan) by using an R-AXIS IV^{++} system (RIGAKU, Tokyo, Japan) as a detector (*21*). The X-ray

wavelength was tuned to 1.000 Å, and the camera distance was set at 1050 mm. The temperature of the samples was kept at 25°C. A sample cell with the thickness of 3.0 mm was used to maximize scattering of X-ray. The windows of the cell were made of 0.02-mm thick quartz plates. In order to avoid radiation damage, we chose the optimal exposure time for each measurement depending on the concentration of the sample; and the current of the ionization chamber monitoring the intensity of the incident X-ray beam was integrated to normalize scattering intensities. To avoid systematic errors, we measured sample and buffer solutions alternately. Stability of SAXS profiles showed that there was no radiation damage to any of the samples. For each polypeptide, SAXS profiles were collected at the concentrations of 2.5, 5.0, 8.0 and 12.5 mg ml^{-1}. In every series of experiments, SAXS profiles of ovalbumin ($Mr = 45,000$, Sigma) were collected as a reference for molecular weight determination.

Processing and Analyses of SAXS Data—Two-dimensionally recorded scattering patterns were converted to a one-dimensional profile by circular averaging. The profile from a buffer solution was subtracted as the background. Scattering profiles in the small-angle region were analysed by Guinier's approximation for monodispersive systems (*16*): the scattering intensity $I(S,C)$, as a function of the reciprocal vector S and protein concentration C, is expressed by the forward scattering intensity, $I(0,C)$ and the radius of gyration, $R_g(C)$, as

$$I(S,C) = I(0,C) \exp\left[-\frac{4\pi^2}{3} R_g(C)^2 S^2 \right]$$

$$S = \frac{2 \sin \theta}{\lambda}$$

where 2θ is the scattering angle and λ is the X-ray wavelength. The reciprocal vector, S, was calibrated by meridional reflections from chicken tendon collagen. In order to eliminate interparticle interference, we made measurements at four different protein concentrations and then extrapolated these datum points to a zero-protein concentration. Distance distribution functions [$P(r)$] were calculated by the indirect transformation of the scattering profiles by using a GNOM package (*22*). Also, the largest linear distance (D_{max}) was determined by the procedure of Flanagan *et al.* (*23*). In particular, when analysing SAXS profiles with aggregation effects at the innermost scattering angles, this program can eliminate these effects by discarding the datum points in the very small angle regions as carried out in SAXS studies on nucleocytoplasmic transport factors (*24*). Assuming a partial specific volume of 0.73 cm^3/g for soluble proteins, the M_w of a protein is determined by using $I(0,C=0)$ of a reference protein with a known molecular weight. Molecular structures of the polypeptides were predicted by applying the *ab initio* structure determination program GASBOR (*25*) to scattering profiles weighted by S^{-4} to ensure Porod's law in $S < 0.15$ Å^{-1}. Because the *ab initio* simulations do not provide a unique solution for 3D structure, 10 molecular structures of L-PGDS and L-PGDS/ligand complexes were predicted as assemblies of 167 dummy scatterers. The program optimizes the configurations of dummy

scatterers to satisfy simultaneously their compact packing and minimum discrepancy factor χ^2 between the experimental $[I_{\mathrm{exp}}(S)]$ and calculated $[I_{\mathrm{model}}(S)]$ profiles. Discrepancies were examined with the χ^2 values (*24, 26*) defined as

$$\chi^2 = \frac{1}{(N-1)}\sum\left\{\frac{\left[I_{\mathrm{exp}}(S_j) - K_{\mathrm{model}}I_{\mathrm{model}}(S_j)\right]}{\sigma(S_j)}\right\}^2$$

where N is the number of experimental datum points, K_{model} is a scaling factor and $\sigma(S_j)$ is the statistical error of $I_{\mathrm{exp}}(Sj)$ at the scattering vector Sj (*26*). The modeling calculations were repeated until the χ^2 of each model became less than 2.0. The 10 predicted molecular structures having almost the same overall structures were averaged, and then aligned with SUPCOMB (*27*).

Statistical Analysis—Data were expressed as the mean ± standard deviation. The statistical significance between the control and the experimental group was assessed by Student's *t*-test. $P < 0.05$ was considered to be significant.

RESULTS AND DISCUSSIONS

Binding Affinity of L-PGDS, βLG and RBP for Small Lipophilic Ligands—We first measured the ability of lipophilic ligands to bind L-PGDS by conducting an intrinsic tryptophan fluorescence quenching assay. L-PGDS showed fluorescence quenching of intrinsic tryptophan residues to occur in a concentration-dependent manner after the addition of RA, BR or BV (Fig. 1A). In a previous study, the results of a fluorescence quenching assay revealed that both Trp43 and Trp54 residues contributed to the fluorescence quenching of L-PGDS due to the binding of a hydrophobic ligand (*15*). The fluorescence intensity decreased to less than 13, 10 and 14% of that of L-PGDS itself in the presence of 10 μM RA, BV and BR, respectively. The K_d values of L-PGDS were calculated from the quenching curves to be 138 ± 8 nM for RA, 103 ± 5 nM for BR and 70 ± 7 nM for BV, respectively (Table 1). Two other members of the lipocalin family, βLG and RBP, also showed concentration-dependent fluorescence quenching after the addition of RA (Fig. 1B and C). The fluorescence intensities of both proteins decreased to 55% in the presence of 10 μM RA, and the K_d values were calculated to be 122 ± 13 nM for βLG and 108 ± 6 nM for RBP (Table 1). βLG contains two tryptophan residues at positions 19 and 61. The Trp19 residue is located at the bottom loop of the hydrophobic pocket and faces the inside of the pocket, whereas the Trp61 residue locates on the C β-strand and faces the outside of the hydrophobic pocket (*28*). In case of βLG, only Trp19 is considered to contribute to the fluorescence quenching because almost half of the fluorescence was quenched in the presence of the excess amount of RA. Bovine RBP contains four tryptophan residues at positions 24, 67, 91 and 105. The Trp24 residue is located on the A β-strand at the bottom of the hydrophobic pocket and faces the inside of the pocket, whereas the Trp67, Trp91 and Trp105 residues locate on the CD loop position, E β-strand and F β-strand, respectively, and these three tryptophan residues face the outside of the hydrophobic pocket (*29*). In case of RBP, at least Trp24 is
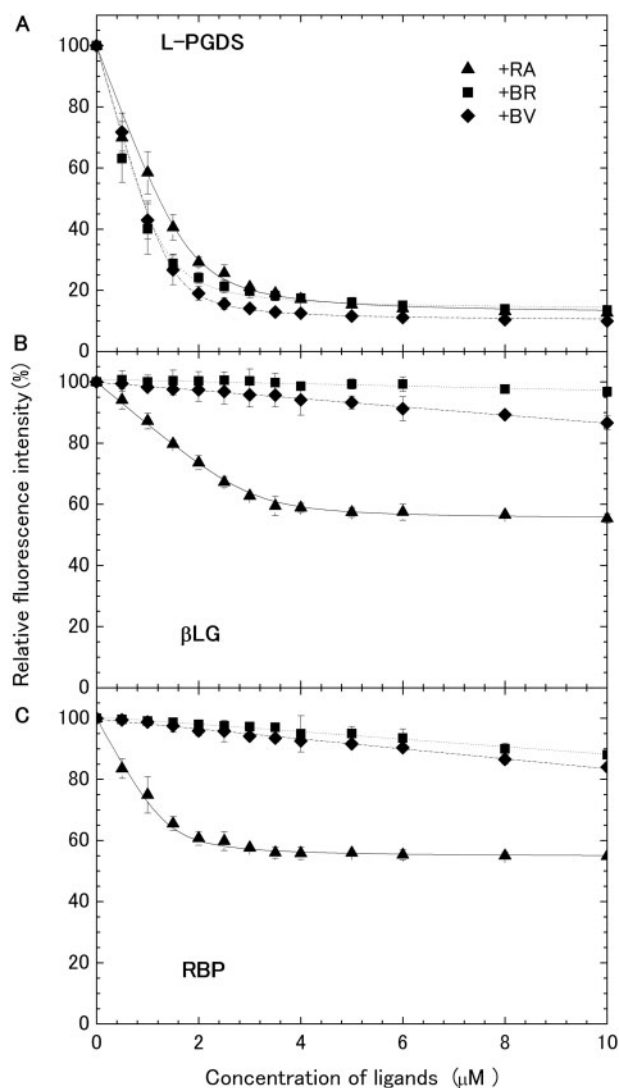

Fig. 1. **Tryptophan fluorescence quenching of (A) L-PGDS, (B) βLG and (C) RBP by small lipophilic ligands.** The concentration of each protein was adjusted to 1.5 μM. The relative fluorescence intensities of L-PGDS, βLG and RBP in the presence of various concentrations of all-*trans*-retinoic acid (RA) (filled triangle with solid line), bilirubin (BR) (filled square with dotted line) and biliverdin (BV) (filled diamond with dot-dashed line) were obtained. Data are expressed as mean ± SE of three independent experiments.

considered to contribute to the fluorescence quenching. In the presence of 10 μM BV or BR, however, the fluorescence intensities of βLG and RBP were still remained more than 85%, indicating that these two lipocalins do not bind BV or BR to the same binding pocket used for RA. These results, taken together, demonstrate that L-PGDS exhibited high binding affinities for RA, BV and BR and a broad selectivity for small lipophilic ligands as compared with βLG and RBP.

The molecular structure of C89A/C186A-substituted L-PGDS obtained from NMR analysis revealed that there is a short 3_{10} helix on the edge of the β-barrel and that the Trp54 residue is located in this helix, whereas Trp43 residue is located at the bottom of the

Table 1. **Binding affinities of L-PGDS, βLG and RBP for RA, BR and BV, and changes in R_g and molecular weights of these proteins induced by the binding of different ligands.**

	K_d (nM)	$R_g(0)$ (Å)	$I(0,0)$	Molecular weight (Da)
L-PGDS	–	19.4 ± 0.03	777 ± 8	2.1×10^4
L-PGDS/RA	138 ± 8	18.8 ± 0.10	759 ± 8	2.0×10^4
L-PGDS/BR	103 ± 5	17.3 ± 0.12	780 ± 5	2.1×10^4
L-PGDS/BV	70 ± 7	17.8 ± 0.04	803 ± 3	2.1×10^4
βLG	–	20.3 ± 0.16	781 ± 4	2.1×10^4
βLG/RA	122 ± 13	20.5 ± 0.27	784 ± 1	2.1×10^4
RBP	–	26.2 ± 0.28	812 ± 4	2.1×10^4
RBP/RA	108 ± 6	26.7 ± 0.23	874 ± 1	2.1×10^4

hydrophobic cavity (30). In addition, it has been recognized that Trp54 on the helix faces the outside of the molecule; and a fluctuation of the helix was found. The fluorescence quenching of L-PGDS should be caused by the interaction between the ligand molecule and these two tryptophan residues. Therefore, we propose that a conformational change in the molecule led to the movement of these tryptophan residues and thus changed the interaction between those residues and the ligand molecule, resulting in the fluorescence quenching.

SAXS Analysis of L-PGDS, βLG and RBP—We then determined the SAXS of L-PGDS, βLG and RBP in the presence or the absence of those lipophilic ligands to investigate the structural changes caused by the ligand binding (Fig. 2). The scattering intensity curves of L-PGDS in the presence or absence of ligands showed a large central peak at a reciprocal vector $(S) < 0.032\,\text{Å}^{-1}$, a second peak at $S = 0.044\,\text{Å}^{-1}$ and a small maximum at $S = 0.075\,\text{Å}^{-1}$. These curves revealed that L-PGDS has a globular shape in the presence or absence of ligands.

The binding of ligand to L-PGDS caused clear changes in the scattering curve only in the small-angle region $(S < 0.02\,\text{Å}^{-1}$, Fig. 2A *inset*) but had no effect on the curves in the other regions. The innermost part of SAXS profiles is sensitive to the overall size and geometry of domain structures. Therefore, we evaluated the radius of gyration $R_g(C)$ by performing Guinier plot analysis of the scattering curves. The Guinier plot at different concentrations of L-PGDS (Fig. 3A) showed a single linear regression line without significant upward curvature even at the low S^2 region, indicating that the sample solution was mono-dispersed without aggregation in the solution at the highest concentration $(12.5\,\text{mg ml}^{-1})$. The Guinier plot of the SAXS data obtained from L-PGDS-ligand complexes also showed the same feature as that in the absence of ligand (data not shown). The apparent $R_g(C)$ and the normalized forward intensity $[I(0,C)]$ of L-PGDS and its ligand-complexes were calculated from the slope and intercept, respectively, of the linear fits of the single regression line of the Guinier plot.

When the calculated $R_g(C)^2$ and $I(0,C)/C$ values were plotted as a function of the protein concentration (Fig. 3B and C), values obtained from both L-PGDS and its complexes with RA, BR and BV showed a linear concentration-dependency, indicating the nature of
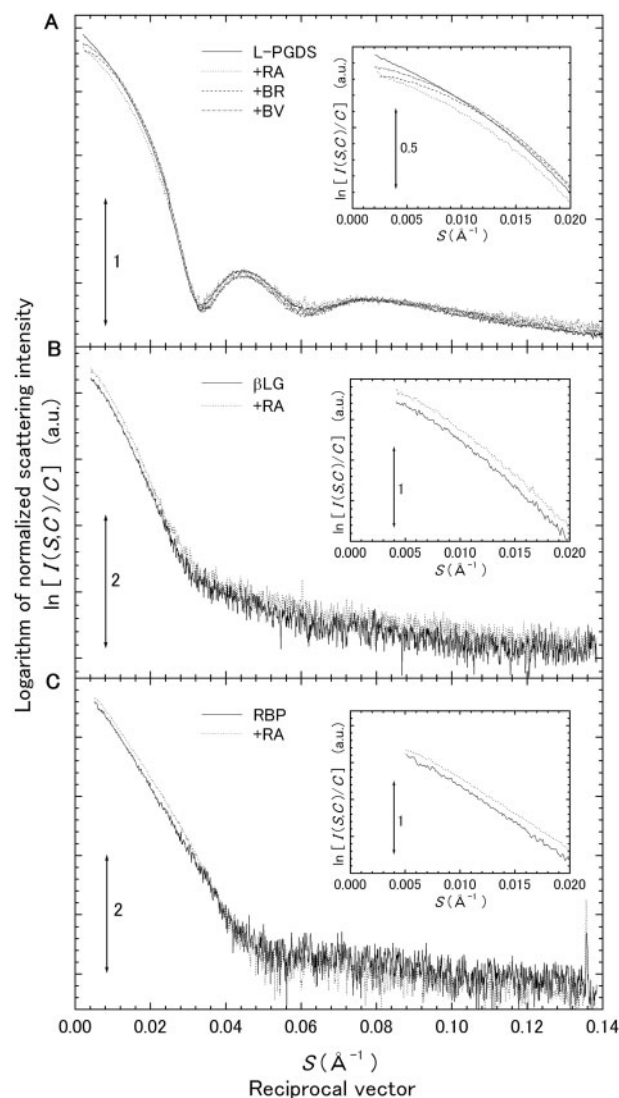

Fig. 2. **(A) SAXS profiles of L-PGDS and each L-PGDS complex.** SAXS profiles of L-PGDS (solid line), L-PGDS/RA (dotted line), L-PGDS/BR (dashed line) and L-PGDS/BV (dot-dashed line) are shown. (B) SAXS profiles of βLG and βLG complexed with RA. SAXS profiles of βLG (solid line) and βLG/RA (dotted line) are shown. (C) SAXS profiles of RBP and RBP complexed with RA. SAXS profiles of RBP (solid line) and RBP/RA (dotted line) are shown. The logarithm of scattering intensity is shown as a function of reciprocal vector (S). Each inset shows the logarithm of scattering intensity in the small S region.

interparticle interferences. The slope of this plot (Fig. 3B) corresponded to the second virial coefficient, and the negative slope indicated the attractive interactions between L-PGDS molecules. The slope of the concentration-dependent curves of $R_g(C)^2$ and $I(0,C)/C$ was slightly different for each sample.

From the linear extrapolations of $R_g(C)^2$ to infinite dilution, which eliminated interparticle interferences, $R_g(0)$ was calculated to be $19.4 \pm 0.03\,\text{Å}$ for L-PGDS, $18.8 \pm 0.10\,\text{Å}$ for L-PGDS/RA, $17.3 \pm 0.12\,\text{Å}$ for L-PGDS/BR and $17.8 \pm 0.04\,\text{Å}$ for L-PGDS/BV (Table 1), indicating

Fig. 4. **The distance distribution functions [$P(r)$] of L-PGDS with different ligands (without ligand, solid line; +RA, dotted line; +BR, dashed line; +BV, dot-dashed line).** The curves were calculated from the SAXS profiles of each protein.
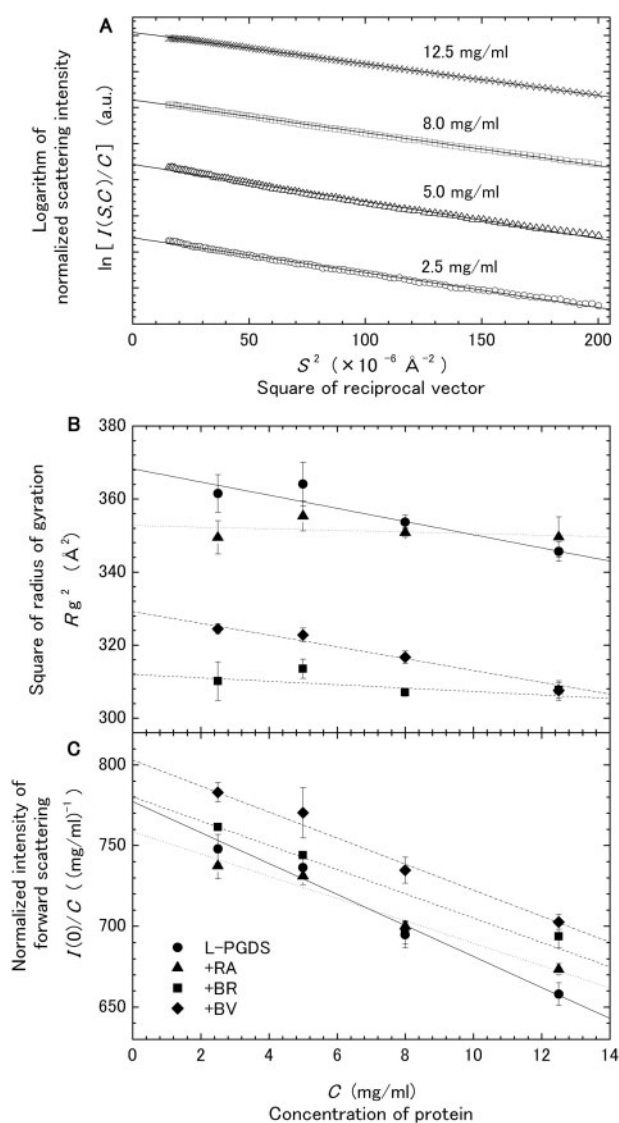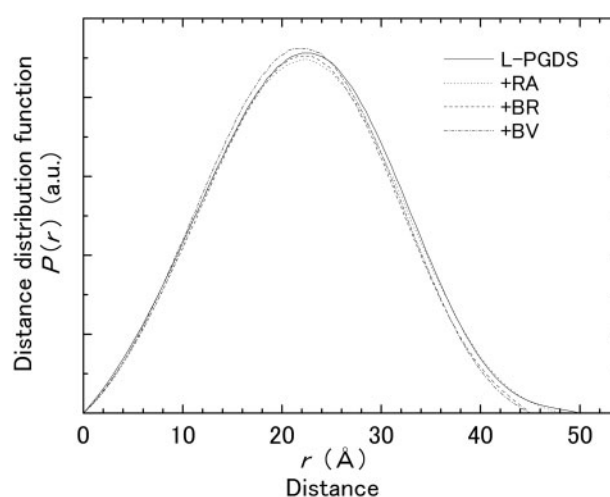
Fig. 3. **Examples of the analysis of data obtained from SAXS experiments.** Example of Guinier plots (A) Logarithms of intensities plotted against squared scattering vector length of L-PGDS at concentrations of 2.5 mg/ml (open circle), 5.0 mg/ml (open triangle), 8.0 mg/ml (open square) and 12.5 mg/ml (×) are shown. They have been shifted along the ordinate for clarity. Concentration dependence of R_g^2 (B) and $I(0,C)/C$ (C) of L-PGDS with and without different ligands is shown (without ligand: filled circle, +RA, filled triangle; +BR, filled square; +BV, filled diamond). Data are expressed as the mean ± SD of three independent experiments.

that L-PGDS became compact after binding these ligands.

The molecular weights of L-PGDS and its complexes with the ligands were calculated to be 2.0×10^4 – 2.1×10^4 Da from the linear relation between the forward scattering intensity and the molecular weight of the protein (Table 1). These values are in good agreement with the molecular weight of L-PGDS calculated from its amino acid sequence (1.9×10^4 Da).

We also calculated distance distribution functions [$P(r)$] from the SAXS curves. The profile of $P(r)$ values

of L-PGDS showed a single peak at 22 Å of distance and was very similar in the presence and absence of any of the three ligands (Fig. 4). These results indicate that the L-PGDS molecule possesses a globular shape and that its overall shape is maintained after binding those ligands. The R_g value of each sample was calculated from $P(r)$ to be 17.2 ± 0.04 Å for L-PGDS, 16.9 ± 0.01 Å for L-PGDS/RA, 16.8 ± 0.01 Å for L-PGDS/BR and 16.9 ± 0.01 Å for L-PGDS/BV, indicating that L-PGDS became compact after binding these ligands. These results obtained from $P(r)$ show the same tendency to become smaller upon the ligand binding as those obtained from the Guinier approximation (Table 1). The calculated largest linear distance (D_{max}) of the three complexes was smaller than that of L-PGDS, that is, 50 Å for L-PGDS, 48 Å for L-PGDS/RA, 45 Å for L-PGDS/BR and 45 Å for L-PGDS/BV. These results also indicate that the molecular structures of the L-PGDS/ligand complexes were more compact than that structure of L-PGDS without a ligand.

In the cases of SAXS measurements on βLG and RBP, the SAXS profiles were the same in the presence and absence of RA (Fig. 2B and C). The calculated $R_g(0)$ values were estimated to be 20.3 ± 0.16 Å for βLG, 20.5 ± 0.27 Å for βLG/RA, 26.2 ± 0.28 Å for RBP and 26.7 ± 0.23 Å for RBP/RA (Table 1), suggesting that the size of both βLG and RBP was almost the same before and after binding of RA.

Molecular Structure of L-PGDS Before and After Binding Ligands—All data from the SAXS analyses revealed that L-PGDS molecule became smaller upon ligand binding. To visualize the structure of L-PGDS and complexes, we calculated the molecular models of them by using the *ab initio* method GASBOR (25). The *ab initio* model of L-PGDS showed that the overall structure of molecule was globular in shape (Fig. 5A). To confirm the adequacy of the *ab initio* model, we compared the molecular structure of C65A-substituted
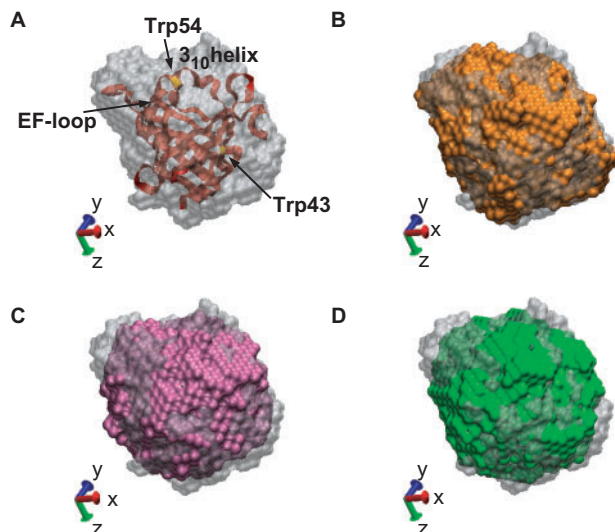
Fig. 5. The *ab initio* model of L-PGDS, L-PGDS/RA, L-PGDS/BR and L-PGDS/BV and the comparison of molecular models. (A) the crystal structure of L-PGDS (a ribbon model) is superimposed on the *ab initio* model of L-PGDS (gray-coloured transparent model). Arrows show the positions of EF-loop and two tryptophan residues, Trp43 and Trp54. (B) The *ab initio* model of L-PGDS/RA (yellow-coloured model) is superimposed on that of L-PGDS (gray-coloured transparent model). (C) The *ab initio* model of L-PGDS/BR (pink-coloured model) is superimposed on that of L-PGDS (gray-coloured transparent model). (D) The *ab initio* model of L-PGDS/ BV (green-coloured model) is superimposed on that of L-PGDS (gray-coloured transparent model). Each *ab initio* model was calculated from $P(r)$ functions by using GASBOR. The χ^2 of each model was less than 2.0. The ribbon model is drawn based on the crystallographic data that could be found in the Protein Data Bank (PDB code 2CZU; Kumasaka, T. *et al.*, 2006, personal communication).

L-PGDS obtained by X-ray crystallography found in the Protein Data Bank (PDB code 2CZU; T. Kumasaka *et al.*, 2006, personal communication) with the *ab initio* model. As these two models fit one another well, we concluded the predicted molecular model to be reasonable (Fig. 5A). Furthermore, in order to compare the shapes between L-PGDS and complexes, we superimposed each model of complex onto that of L-PGDS. The other three models of complexes also had globular shapes, and they became more compact than L-PGDS upon ligand binding (Fig. 5B, C and D). Although it should be kept in mind that each model is not a unique solution as would be obtained by X-ray crystallography, we consider that the packing of the complexed molecules had been induced certainly by the ligand binding. Our data also revealed that the magnitude of the compactness might depend on the size of the ligand which bound to L-PGDS. We considered that those results indicated directly the structural flexibility of L-PGDS molecule. This idea might be also supported by the fact, such as unchanged R_g values and incomplete fluorescence quenching in the cases of two other lipocalins. Such the structural flexibility might be due to the distinguishing molecular structure of L-PGDS itself and the origin of the compact packing observed only on the L-PGDS. On the other hand, the NMR analysis of C89A/C186A-substituted

L-PGDS revealed that the inside cavity of L-PGDS had an unusually bifurcated shape and a larger entry than those in other lipocalins. This study also suggested that such the unusually shaped large cavity of L-PGDS make it possible to bind bulky ligands, such as BR or BV and lead the feature of the broad selectivity of the ligand binding (*30*). Based on these facts, we consider that these structural uniqueness leads for only L-PGDS to possess the ability to bind the variety of ligands with the high binding affinity in a different manner from many other lipocalin proteins. Eventually, we propose the model for the binding of the ligands to L-PGDS as follows; a lipophilic ligand enters the large cavity of the β-barrel, which triggers a conformational change such that the molecule of L-PGDS becomes compact; and thus the ligand is held tightly inside the L-PGDS molecule.

CONFLICT OF INTEREST

None declared.

REFERENCES

1. Urade, Y. and Eguchi, N. (2002) Lipocalin-type and hematopoietic prostaglandin D synthases as a novel example of functional convergence. *Prostaglandins Other Lipid Mediat.* **68–69**, 375–382
2. Toh, H., Kubodera, H., Nakajima, N., Sekiya, T., Eguchi, N., Tanaka, T., Urade, Y., and Hayaishi, O. (1996) Glutathione-independent prostaglandin D synthase as a lead molecule for designing new functional proteins. *Protein Eng.* **9**, 1067–1082
3. Flower, D.R., North, A.C., and Sansom, C.E. (2000) The lipocalin protein family: structural and sequence overview. *Biochim. Biophys. Acta* **1482**, 9–24
4. Beynon, R.J. and Hurst, J.L. (2004) Urinary proteins and the modulation of chemical scents in mice and rats. *Peptides* **25**, 1553–1563
5. Briand, L., Trotier, D., and Pernollet, J.C. (2004) Aphrodisin, an aphrodisiac lipocalin secreted in hamster vaginal secretions. *Peptides* **25**, 1545–1552
6. Breustedt, D.A., Korndorfer, I.P., Redl, B., and Skerra, A. (2005) The 1.8-A crystal structure of human tear lipocalin reveals an extended branched cavity with capacity for multiple ligands. *J. Biol. Chem.* **280**, 484–493

7. Ganforina, M.D., Gutiérrez, G., Bastiani, M., and Sanchez, D. (2000) A phylogenetic analysis of the lipocalin protein family. *Mol. Biol. Evol.* **17**, 114–126

8. Cowan, S.W., Newcomer, M.E., and Jones, T.A. (1990) Crystallographic refinement of human serum retinol binding protein at 2 Å resolution. *Proteins Struct. Funct. Genet.* **8**, 44–61

9. Urade, Y., Fujimoto, N., and Hayaishi, O. (1985) Purification and characterization of rat brain prostaglandin D synthetase. *J. Biol. Chem.* **260**, 12410–12415

10. Tanaka, T., Urade, Y., Kimura, H., Eguchi, N., Nishikawa, A., and Hayaishi, O. (1997) Lipocalin-type prostaglandin D synthase (beta-trace) is a newly recognized type of retinoid transporter. *J. Biol. Chem.* **272**, 15789–15795

11. Beuckmann, C.T., Aoyagi, M., Okazaki, I., Hiroike, T., Toh, H., Hayaishi, O., and Urade, Y. (1999) Binding of biliverdin, bilirubin, and thyroid hormones to lipocalin-type prostaglandin D synthase. *Biochemistry* **38**, 8006–8013

12. Inui, T., Ohkubo, T., Urade, Y., and Hayaishi, O. (1999) Enhancement of lipocalin-type prostaglandin D synthase enzyme activity by guanidine hydrochloride. *Biochem. Biophys. Res. Commun.* **266**, 641–646

13. Mohri, I., Taniike, M., Okazaki, I., Kagitani-Shimono, K., Aritake, K., Kanekiyo, T., Yagi, T., Takikita, S., Kim, H. S., Urade, Y., and Suzuki, K. (2006) Lipocalin-type prostaglandin D synthase is up-regulated in oligodendrocytes in lysosomal storage diseases and binds gangliosides. *J. Neurochem.* **97**, 641–651

14. Kanekiyo, T., Ban, T., Aritake, K., Huang, Z.L., Qu, W.M., Okazaki, I., Mohri, I., Murayama, S., Ozono, K., Taniike, M., Goto, Y., and Urade, Y. (2007) Lipocalin-type prostaglandin D synthase/beta-trace is a major amyloid beta-chaperone in human cerebrospinal fluid. *Proc. Natl Acad. Sci. USA* **104**, 6412–6417

15. Inui, T., Ohkubo, T., Emi, M., Irikura, D., Hayaishi, O., and Urade, Y. (2003) Characterization of the unfolding process of lipocalin-type prostaglandin D synthase. *J. Biol. Chem.* **278**, 2845–2852

16. Guinier, A. and Fournet, G. (1955) *Small-Angle Scattering of X-rays*, John Wiley, New York

17. McDonagh, A.F. and Assisi, F. (1971) Commercial bilirubin: A trinity of isomers. *FEBS Lett.* **18**, 315–317

18. McPhee, F., Caldera, P.S., Bemis, G.W., McDonagh, A.F., Kuntz, I.D., and Craik, C.S. (1996) Bile pigments as HIV-1 protease inhibitors and their effects on HIV-1 viral maturation and infectivity *in vitro*. *Biochem. J.* **320**, 681–686

19. Liu, R.S.H. and Asato, A.E. (1982) Synthesis and photochemistry of stereoisomers of retinal. *Methods Enzymol.* **88**, 506–516

20. Cogan, U., Kopelman, M., Mokady, S., and Shinitzky, M. (1976) Binding affinities of retinol and related compounds to retinol binding proteins. *Eur. J. Biochem.* **65**, 71–78

21. Inoue, K., Oka, T., Miura, K., and Yagi, N. (2004) Present status of BL40B2 and BL40XU at SPring-8 (Beamlines for small angle X-ray scattering). *AIP Conf. Proc.* **705**, 336–339

22. Svergun, D.I. (1992) Determination of the regularization parameter in indirect-transform methods using perceptual criteria. *J. Appl. Crystallogr.* **25**, 495–503

23. Flanagan, J.M., Kataoka, M., Fujisawa, T., and Engelman, D.M. (1993) Mutations can cause large changes in the conformation of denatured protein. *Biochemistry* **32**, 10359–10370

24. Fukuhara, N., Fernandez, E., Ebert, J., Conti, E., and Svergun, D.I. (2004) Conformational variability of nucleo-cytoplasmic transport factor. *J. Biol. Chem.* **279**, 2176–2181

25. Svergun, D.I., Petoukhov, M.V., and Koch, M.H.J. (2001) Determination of domain structure of proteins from X-ray solution scattering. *Biophys. J.* **80**, 2946–2953

26. Svergun, D.I. (1999) Restoring low resolution structure of biological macromolecules from solution scattering using simulated annealing. *Biophys. J.* **76**, 2879–2886

27. Kozin, M.B. and Svergun, D.I. (2001) Automated matching of high- and low-resolution structural models. *J. Appl. Crystallogr.* **34**, 33–41

28. Wu, S.Y., Perez, M.D., Puyol, P., and Sawyer, L. (1999) Beta-lactoglobulin binds palmitate within its central cavity. *J. Biol. Chem.* **274**, 170–174

29. Calderone, V., Berni, R., and Zanotti, G. (2003) High-resolution structures of retinol-binding protein in complex with retinol: pH-induced protein structural changes in the crystal state. *J. Mol. Biol.* **329**, 841–850

30. Shimamoto, S., Yoshida, T., Inui, T., Gohda, K., Kobayashi, Y., Fujimori, K., Tsurumura, T., Aritake, K., Urade, Y., and Ohkubo, T. (2007) NMR solution structure of lipocalin-type prostaglandin D synthase: evidence for partial overlapping of catalytic pocket and retinoic acid-binding pocket within the central cavity. *J. Biol. Chem.* **282**, 31373–31379